

DESIGN AND ANALYSIS OF A MULTI-CARRIER TX-RX SYSTEM BASED ON RATIONALLY SYNCHRONIZED OSCILLATORS FOR LOCALIZATION APPLICATIONS

M. Fernandez*, S. Ver Hoeye, C. Vazquez, G. Hotopan, R. Camblor, and F. Las Heras

Area of Signal Theory and Communications, Department of Electrical Engineering, University of Oviedo, Campus de Viesques, Edificio Polivalente s/n, Modulo 8, Planta 1, E-33203, Gijon, Spain

Abstract—In this work, a novel multi-carrier *Tx-Rx* system based on rationally synchronized oscillators to be used in RF-source localization applications is presented. The *Tx* subsystem is composed by two rationally synchronized oscillators, with different operation frequency, which share the reference signal. This signal is transmitted together with the one generated by the oscillators. In the *Rx* subsystem, the reference signal is provided by an oscillator which is synchronized with the received reference signal. According to the simulation results, with the proposed approach, the determination of the relative phase variation suffered by the transmitted signals, due to the propagation channel, can be achieved with an error less than 0.6° . It is also shown that the dynamic response of the system can be optimized by properly selecting the operation point of all oscillators.

1. INTRODUCTION

During the last years, several techniques for RF-based indoor localization systems [1–4] have been developed. Some of them are based on the determination of the direction of arrival (DoA) [5–7] or the time of arrival (ToA) [8], but in both cases, multipath effects reduce their efficiency. In order to overcome this drawback, other techniques consider the strength of the received signals [9] and use triangulation methods in order to determine the position of the transmitters. Although these methods present a good accuracy, a great effort has been carried out for developing numerical techniques

Received 15 July 2011, Accepted 25 August 2011, Scheduled 27 August 2011

* Corresponding author: Miguel Fernandez Garcia (mfgarcia@tsc.uniovi.es).

to improve it [8,10]. From the hardware point of view, the target positioning accuracy can be enhanced if information about both magnitude and phase of several transmitted signals is available in the receivers [11].

The most common topologies used in order to design coherent multi-carrier transmitters and receivers with a common phase reference are based on Phase-Locked Loops (PLL) [12]. PLL-based systems have desirable characteristics such as their dynamical response, capability to determine phase variations with high accuracy, and good frequency and phase stability. However, when several carrier signals are needed, the complexity and the cost of these systems greatly increases with the number of used PLLs.

A novel approach to design a *Tx-Rx* multicarrier system with capability of phase variation determination, based on Rationally Synchronized Oscillators (RSO) [13,14], is described in this paper. The RSO is a very compact and low cost circuit, since it is based on a single transistor and a reduced number of components. The proposed system provides the same advantages as a PLL-based system [13], with lower complexity and cost.

A coherent two carrier system is designed and analyzed. On the one hand, the transmitter subsystem is composed by two RSO circuits synchronized with a common reference signal with frequency $f_r = 5$ GHz. Each RSO generates a carrier signal with different frequency, $f_{o,\frac{3}{5}} = 3$ GHz, $f_{o,\frac{3}{4}} = 3.75$ GHz. These two signals are transmitted along with a sample of the reference signal. As the two oscillators are injection-locked with the same reference signal, the transmitted signals have a fixed known phase relation which is reached through their synchronizing harmonic components.

On the other hand, the receiver topology is similar to the transmitter one. It is based on two RSO which are identical to those used in the transmitter. In this case, their reference signal is provided by an oscillator that is synchronized with the received reference signal. The relative phase variation suffered by the transmitted signals, due to the arbitrary propagation channel, will be calculated by comparing the phase of the received signals and the phase of the signals generated in the *Rx* RSOs.

The described system is analyzed through nonlinear harmonic balance and envelope transient techniques based on the use of auxiliary generators [13,15–17]. The advantages of using an additional oscillator in the *Rx* subsystem will be shown, and the main error sources will be identified. Finally, it will be demonstrated that the relative phase variation of the transmitted signals can be calculated with an error less than 0.6° .

2. DESIGN AND ANALYSIS OF THE TRANSMITTER

2.1. Topology

The topology of the transmitter is depicted in Fig. 1. Part (a) shows the schematic of the individual RSO. It is based on a single P-HEMT transistor with a feedback network placed at the source port which provides the start-up oscillation condition. It includes a varactor diode to modify the frequency of the self-oscillation signal. The input reference signal is connected to the RSO through a band-pass filter, with central frequency f_r , placed at the gate port of the transistor, and the output signal, with frequency f_o is selected at the drain port by means of a band-pass filter. A multi-harmonic load based on an arbitrarily width modulated microstrip transmission line [18, 19], which is used for optimization purposes, is also connected at the gate port of the transistor.

Under synchronized operation, the N th harmonic component of the autonomous signal synchronizes with the M th harmonic component of the input reference signal, which is generated due to the nonlinear characteristic of the active element. Therefore, the rational ratio between the input and output signals can be expressed as $r = \frac{M}{N} = \frac{f_o}{f_r}$, and there exists a fixed known relation between their phase.

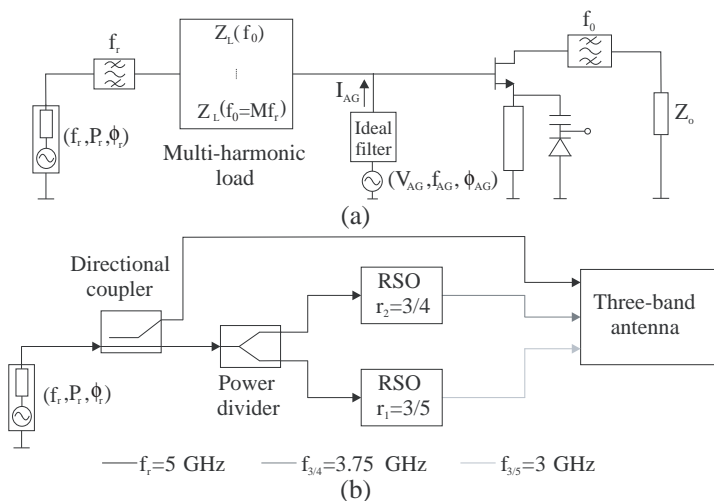


Figure 1. (a) Topology of the individual RSO with inclusion of an auxiliary generator for optimization purposes. (b) Topology of the RSO based transmitter.

Figure 1(b) shows the topology of the multi-carrier transmitter, composed by two RSOs synchronized with the same reference signal, with frequency $f_r = 5$ GHz, power P_r and phase ϕ_r . This signal is provided to each oscillator by means of a power divider which is designed in order to ensure that the reference signal available at the input is identical for all RSOs. Since the frequency of the self-oscillation signal of each RSO is different, $f_{o, \frac{3}{5}} = 3$ GHz and $f_{o, \frac{3}{4}} = 3.75$ GHz, the rational relation r_i must also be different:

$r_1 = \frac{f_{o, \frac{3}{5}}}{f_r} = \frac{M}{N_1} = \frac{3}{5}$, $r_2 = \frac{f_{o, \frac{3}{4}}}{f_r} = \frac{M}{N_2} = \frac{3}{4}$. In this way, it is possible to generate two signals with non-harmonical frequency ratio and with a known phase relation with the reference signal, as shown in Equations (A1) to (A8) in Appendix A. Together with the output signals of the RSOs, a sample of the reference signal is transmitted by means of a three port multi-band antenna [20–23].

Note that the proposed architecture is easily scalable, by simply adding the desired number of RSO circuits, with the proper rotation number $r_i = \frac{M}{N_i}$.

2.2. Design and Analysis of the Individual RSO

The frequency $f_{o, \frac{M}{N}}$, the quality factor Q_L and the harmonic content of the circuit are imposed by means of an harmonic balance based optimization process in which several parameters of the circuit are modified in order to satisfy the non-perturbation condition of the auxiliary generator [16, 17], which operates with frequency $f_{AG} = f_{o, \frac{M}{N}}$, amplitude $V_{AG} = V_o^1$ and phase ϕ_{AG} . The synchronization bandwidth is maximized through the control of the harmonic content of the RSO [14], i.e., the amplitudes of the N th harmonic component of the self-oscillation signal, V_o^N and the M th harmonic component of the reference signal, V_r^M , with phase $\phi_{\frac{M}{N}}^N$ and ϕ_r^M , respectively. The use of this technique provides a locking range large enough to ensure that the circuit has practical applications with low reference signal power, and for high synchronization orders, with $M, N > 2$.

The locking range is calculated by tracing the synchronization loci of the circuit. This trace represents all the solutions in which the frequencies of the N th harmonic component of the self-oscillation signal and the M th harmonic component of the reference signal are the same and, thus, the phase difference $\Delta\phi = \phi_r^M - \phi_{\frac{M}{N}}^N$ is constant in time. Assuming that ϕ_r^M is constant, the loci is obtained carrying out a sweep in $\phi_{\frac{M}{N}}^1 = \phi_{AG}$ between 0° and $\frac{360^\circ}{N}$, calculating for

each point of the sweep the values of $f_{AG} = f_o$ and $V_{AG} = V_o^1$ for which the non-perturbation condition of the auxiliary generator is satisfied [16,17]. Fig. 2 shows the synchronization loci of the two RSO with $r_1 = \frac{3}{5}$ and $r_2 = \frac{3}{4}$, obtained with a power value of the reference signal $P_r = -10$ dBm. It is also represented the phase relation $\Delta\phi = \phi_{AG}$ between the first harmonic component of the self-oscillation signal of each RSO and the reference signal. Note that the maximum phase variation is $\frac{360}{N_i}^\circ$, since the first harmonic component of the self-oscillation signal is being considered. Continuous traces correspond to stable solutions, while unstable ones are depicted with dashed line. The stability of the solutions has been determined through the envelope transient technique [16, 17].

2.3. Operation Point of the RSOs

Since the two RSO share the reference signal, their synchronization ranges must be partially overlapping. The optimum operation point of the RSOs is located about the center of the synchronization range. On the one hand, in Fig. 3 it has been represented the dynamic response of the output signal phase change when a 10° step is introduced in the phase of the input reference signal ϕ_r . The time response has been calculated for two different operation points through the envelope transient technique. As can be observed, the response of the oscillator is faster when its operation point is located around the center of its locking range. On the other hand, if the working point is near to the limits of the synchronization range, the system is affected by strong noise amplification due to nonlinear effects [24]. The inclusion

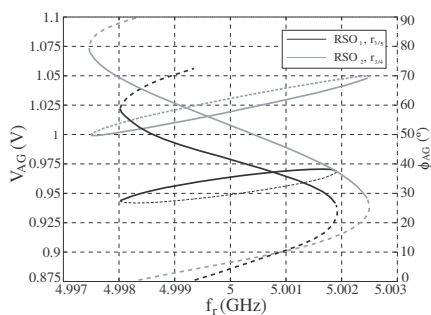


Figure 2. Synchronized solutions of the individual RSOs. Continuous line: stable solutions. Dashed line: unstable solutions.

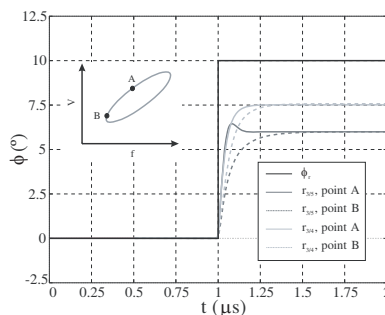


Figure 3. Phase response of the two RSO to a 10° step in ϕ_r .

of a varactor diode as a part of the feedback networks allows the self-oscillation signal frequency tuning, which means that the center frequency of each synchronization loci can be slightly modified, in order to overlap their center points.

2.4. Analysis of the Whole Transmitter

Although the frequency of the reference signal f_r is constant, a complete analysis is performed in order to characterize the behavior of the transmitter shown in Fig. 1(b). The synchronization loci of the two RSO, when the whole system is considered, can not be traced as was described in the case of the individual RSO because of the failure of the available optimization methods when the phase of any signal is included in the set of optimization variables. In addition, as the two locking ranges are not identical, they can not completely overlap and the proposed harmonic balance configuration fails to converge in all points in which the two RSO are not simultaneously synchronized.

To overcome these problems, the envelope transient technique combined with the use of two auxiliary generators is applied. A sweep is carried out in the frequency of the reference signal f_r . At each point of the sweep, the two auxiliary generators, with frequencies $f_{AG,1} = f_{o,\frac{3}{5}}$ and $f_{AG,2} = f_{o,\frac{3}{4}}$, are connected to the corresponding RSO during a short time in order to initialize the state variables of the oscillators. After disconnecting the auxiliary generators, the state variables of the system evolve in time towards the stable steady state solution. As a result, the Poincare maps associated to the power and phase of the first harmonic component of the output signal of each RSO are calculated [16]. The maps are depicted in Figs. 4(a) and (b). A synchronized solution is represented by a point, which means that the value of the associated variable is constant in time. The unsynchronized solutions appear in the Poincare map as vertical lines, due to the time variation experienced by the considered variable. Since the envelope transient technique takes into account the temporal evolution of the state variables, the Poincare map only contains the part of the synchronization loci corresponding to stable solutions.

3. DESIGN AND ANALYSIS OF THE RECEIVER

3.1. Topology

The topology of the receiver system used to determine the phase variation suffered by the transmitted signals ($f_r = 5$ GHz, $f_{o,\frac{3}{5}} = 3$ GHz, $f_{o,\frac{3}{4}} = 3.75$ GHz) due to the arbitrary propagation channel is

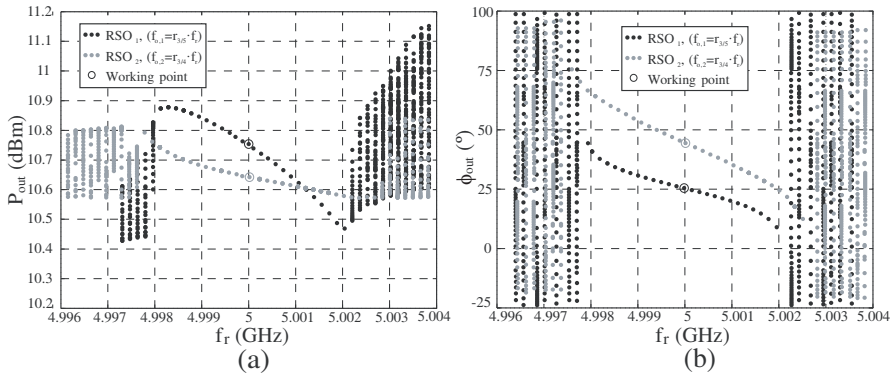


Figure 4. Poincare maps of the multi-carrier transmitter output signals. (a) RSO output power. (b) RSO output phase. The working point of each RSO is remarked.

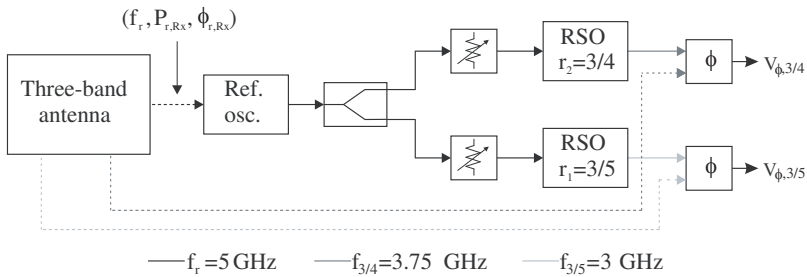


Figure 5. Topology of the receiver. Continuous line: Signals generated by the *Rx* system. Dashed line: Received signals.

shown in Fig. 5. It consists of two RSO identical to those utilized in the transmitter, whose synchronization signal is provided by an additional reference oscillator. This oscillator, with frequency $f_{5,Rx} = f_r = 5$ GHz, is synchronized with the received reference signal, with power $P_{r,Rx}$ and phase $\phi_{r,Rx}$. It is included in the receiver system in order to fix the working point of the two RSOs, which must be identical to the achieved in the transmitter. At the outputs of the power divider which is connected to the reference oscillator, two attenuators are placed in order to ensure that the reference signal power available at the input port of each RSO is $P_{in,RSO} = -10$ dBm.

The received signals at frequency 3 and 3.75 GHz, with phase $\phi_{\frac{3}{5},Rx}$ and $\phi_{\frac{3}{4},Rx}$, are introduced in two phase comparators together with the signals generated in the receiver RSOs, with phase $\phi_{\frac{3}{5},out}$ and

$\phi_{\frac{3}{4},out}$. A DC-voltage proportional to the phase difference between each pair of signals is generated at the output of the comparator. A detailed mathematical description of the whole system operation is provided in Appendix A.

3.2. Reference Oscillator

This oscillator is fundamentally synchronized with the received reference signal, with frequency $f_r = 5$ GHz and phase $\phi_{r,Rx}$. It is designed in order to achieve that the phase of its output signal, $\phi_{5,out}$, is equal to that of their reference signal. Since the output power can be considered as a constant, the reference oscillator ensures that the working point of the RSO is the same as the transmitter, regardless of the power of the received signals.

The Adler equation [25] shows that the locking range of a fundamentally synchronized oscillator is inversely proportional to the amplitude V_o of the self-oscillation signal. Thus, for a given value of the oscillator quality factor Q_L , the minimum reference signal power necessary to achieve a useful synchronization range decreases with V_o . Otherwise, the input reference signal power for which the autonomous signal extinguishes is greater for higher values of V_o . Therefore, the amplitude of the autonomous signal of the reference oscillator must be carefully selected, according to the expected range of the values of received reference signal power $P_{r,Rx}$.

The frequency and the selected value of the amplitude of the self-oscillating signal of the reference oscillator are imposed in the same way as was done in the case of the RSOs, using an auxiliary generator with frequency $f_{AG} = f_r$, amplitude $V_{AG} = V_o$ and phase ϕ_{AG} .

Figure 6 shows the synchronization loci obtained for several values of the input power $P_{r,Rx}$, in terms of the power (a) and the phase (b) of the output signal. Part (b) shows the phase difference $\Delta\phi = \phi_{5,out} - \phi_{r,Rx}$ between the output and input signals, as a function of f_r . As can be observed, for each value of f_r , $\Delta\phi$ depends on the received signal power, except at a point where all traces intersect.

The varactor that is included in the feedback network of the reference oscillator allows the frequency tuning of the autonomous signal and thus, the frequency of the desired working point. In addition, the output network is designed in order to reach zero phase difference between the output and input signals, at the frequency of the reference signal. Therefore, the phase of the reference signal supplied to the RSOs is the same as the received, $\phi_{r,Rx}$, and does not depend on the power of the received reference signal.

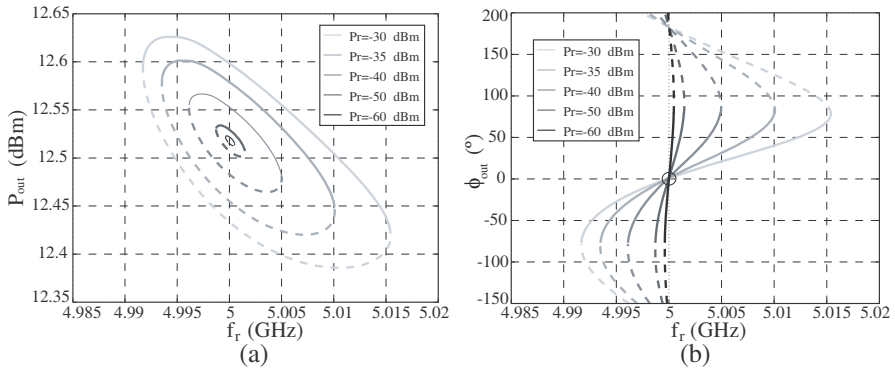


Figure 6. Synchronized solutions of the reference oscillator, in terms of the output signal. (a) Power. (b) Phase. The selected working point is remarked. Continuous traces correspond with stable solutions.

4. ANALYSIS OF THE OVERALL BEHAVIOR OF THE SYSTEM

The characterization of the whole system has been accomplished through the envelope transient technique, because of the failure of the optimization process when finding synchronized solutions, if the phase of any auxiliary generator is considered as part of the optimization variables set.

4.1. Operation Point Errors

The receiver subsystem has been carefully designed in order to ensure that the RSO operation points are identical to those fixed in the transmitter. However, due to the wide range of expected values of the received signals power, a slightly variation of the power and phase of the RSO reference signal provided by the reference oscillator is found.

Despite the selection of the working point indicated in Fig. 6(b), the traces representing the phase variation do not intersect exactly at the same point. This is due to the fact that the frequency of the self-oscillation signal is influenced by the power of the reference signal. Therefore, when a wide range of values of $P_{r,Rx}$ is considered, the traces shown in Fig. 6(b) suffer a small frequency deviation. In order to quantify the magnitude of this error, the phase difference between the output and input signals of the reference oscillator, $\Delta\phi_{5,out} = \phi_{5,out} - \phi_{r,Rx}$ has been represented in Fig. 7, when the received reference signal power varies between -60 and -30 dBm. The

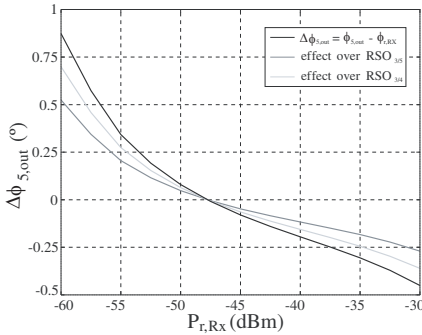


Figure 7. Reference oscillator output signal phase deviation due to the variation of the received synchronization signal power $P_{r,Rx}$.

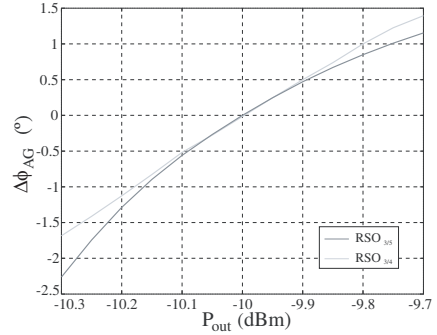


Figure 8. RSO autonomous signal phase error due to the variation of the output power of the reference oscillator.

influence on the phase of the RSO self-oscillation signals has also been represented. Note that the effect on the RSO behavior is weighted by the rational relation r_i .

Other significant error contribution is the variation of the output power of the reference oscillator, related with the jump of the synchronized solutions between the different synchronization loci that occurs when the reference signal power is not constant, as can be observed from the analysis of the stable part of the traces shown in Fig. 6(a), at frequency f_r . The effect of this power variation on the phase of the RSO autonomous signal is represented in Fig. 8. Unlike the case of the reference oscillator, the working point of the RSO can not be adjusted in order to avoid phase variations with the reference signal power because it is high enough to have a great influence on the frequency of the self-oscillation signal and thus, the synchronization loci are not concentric.

4.2. Global Behavior of the Receiver

In order to determine the final error achieved by the receiver, the phase of the output signals of the transmitter RSOs, $\phi_{\frac{3}{5},Tx}$ and $\phi_{\frac{3}{4},Tx}$, has been calculated when the power of the reference source is $P_r = -10$ dBm and its phase is $\phi_r = 0^\circ$. Otherwise, assuming that the phase change of the reference signal due to the propagation channel is $\Delta\phi_{r,H} = 0^\circ$ and, thus, the phase of the received reference signal is $\phi_{r,Rx} = 0^\circ$, the phase of the output signals of the receiver RSOs, $\phi_{\frac{3}{5},out}$

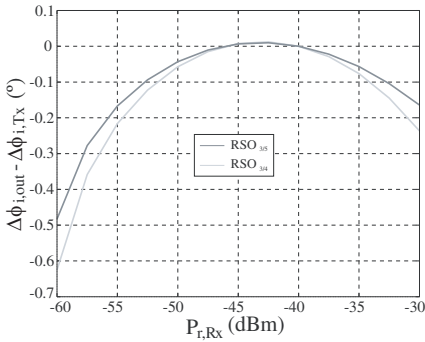


Figure 9. Total receiver RSO output phase error.

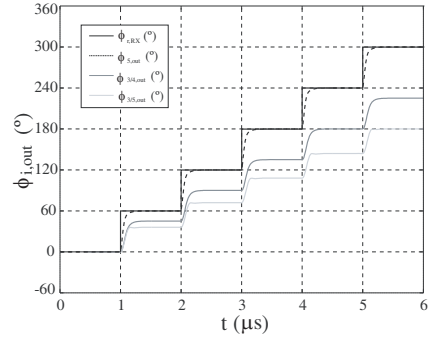


Figure 10. Dynamic response of the receiver.

and $\phi_{\frac{3}{4},out}$ has been calculated. The final error is then calculated as $\Delta\Phi_i = \phi_{i,out} - \phi_{i,Tx}$. The result is shown in Fig. 9. It is observed that the absolute error is less than 0.5° in the case of the signal at 3 GHz, and less than 0.6° in the case of the other RSO, when the received reference signal power suffers a variation between -60 and -30 dBm.

Finally, the dynamic behavior of the receiver has been characterized measuring the output signal phase of each RSO and reference oscillator when several 60° steps are introduced in the received reference signal phase $\phi_{r,Rx}$. The result is shown in Fig. 10. Since the working point of all the oscillators is located about the center of their respective locking ranges, the system reaches an optimum time response.

5. CONCLUSIONS

A new low cost RSO based approach to design a multi-carrier Tx - Rx system with capability of determination the phase change suffered by the transmitted signals due to the arbitrary propagation channel has been presented. The transmitted signals, with frequencies not harmonically related, are generated by two RSO which share the synchronization signal. The reference signal of the receiver is provided by an additional reference oscillator, in order to ensure that the working point of the RSOs is the same as in the transmitter for all the range of expected receiver signals power. The errors in the working point of the Rx RSOs, due to the variation of the received reference signal power have been calculated and it has been demonstrated that the phase variation of the transmitted signals can be determined with an error less than 0.6° . In addition, since the working point of all the

oscillators is located around the center of their synchronization loci, the system provides an optimum time response.

ACKNOWLEDGMENT

This work has been supported by the Ministerio de Ciencia e Innovacion of Spain (FEDER) under projects TEC2008-01638, CONSOLIDER-INGENIO CSD2008-00068 and grant AP2009-0438, by the Gobierno del Principado de Asturias (PCTI/FEDER-FSE) under projects EQUIP08-06, FC09-COF09-12, EQUIP10-31 and PC10-06, grant BP10-031 and by Catedra Telefonica - Universidad de Oviedo.

APPENDIX A.

In a Rationally Synchronized Oscillator (RSO), with rational ratio $r = \frac{f_o}{f_r} = \frac{M}{N}$, the phase of the self-oscillation signal, with frequency f_o is related with the phase of the reference signal, with frequency f_r , through their respective N and M harmonic components, with frequency $Nf_o = Mf_r$. Thus, under synchronized operation regime, the following relations are satisfied:

$$\phi_r^3 - \phi_{\frac{3}{4}}^4 = \Delta\phi_{\frac{3}{4}}, \quad \text{with } -180^\circ \leq \Delta\phi_{\frac{3}{4}} \leq 180^\circ \quad (\text{A1})$$

$$\phi_r^3 - \phi_{\frac{3}{5}}^5 = \Delta\phi_{\frac{3}{5}}, \quad \text{with } -180^\circ \leq \Delta\phi_{\frac{3}{5}} \leq 180^\circ \quad (\text{A2})$$

where ϕ_r^3 represents the phase of the 3rd harmonic component of the reference signal, and $\phi_{\frac{3}{4}}^4$ and $\phi_{\frac{3}{5}}^5$ represent the phase of the 4th and 5th harmonic components of the RSO with $r = \frac{3}{4}$ and $\frac{3}{5}$, respectively. Therefore, the phase of the synchronizing harmonics can be written as:

$$\phi_{\frac{3}{4}}^4 = \phi_r^3 - \Delta\phi_{\frac{3}{4}} \quad (\text{A3})$$

$$\phi_{\frac{3}{5}}^5 = \phi_r^3 - \Delta\phi_{\frac{3}{5}} \quad (\text{A4})$$

where $\Delta\phi_{\frac{3}{4}}$ and $\Delta\phi_{\frac{3}{5}}$ are constant in time. If the two RSO of the transmitter represented in Fig. 1(b) are synchronized, the general condition $Nf_o = Mf_r$ is verified. The phase of the RSO output signals is given by:

$$\phi_{\frac{3}{4},Tx} = 2\pi f_{o,\frac{3}{4}} t + \phi_{o,\frac{3}{4}} + \frac{1}{4}\phi_{\frac{3}{4}}^4 \quad (\text{A5})$$

$$\phi_{\frac{3}{5},Tx} = 2\pi f_{o,\frac{3}{5}} t + \phi_{o,\frac{3}{5}} + \frac{1}{5}\phi_{\frac{3}{5}}^5 \quad (\text{A6})$$

where $\phi_{o,\frac{3}{4}}$ and $\phi_{o,\frac{3}{5}}$ correspond with the initial arbitrary phase value of each RSO self-oscillation signal. Replacing (A3) in (A5), and (A4) in (A6), the phase of the transmitted signals can be expressed as:

$$\phi_{\frac{3}{4},Tx} = 2\pi f_{o,\frac{3}{4}}t + \phi_{o,\frac{3}{4}} + \frac{1}{4} \left(\phi_r^3 - \Delta\phi_{\frac{3}{4}} \right) \quad (A7)$$

$$\phi_{\frac{3}{5},Tx} = 2\pi f_{o,\frac{3}{5}}t + \phi_{o,\frac{3}{5}} + \frac{1}{5} \left(\phi_r^3 - \Delta\phi_{\frac{3}{5}} \right) \quad (A8)$$

The transmitted signals, at 3, 3.75 and 5 GHz suffer a phase change denoted by $\Delta\phi_{\frac{3}{5},H}$, $\Delta\phi_{\frac{3}{4},H}$ and $\Delta\phi_{r,H}$, respectively, due to the propagation through an arbitrary channel with transfer function $H(f)$. The phase of the received signals is then:

$$\phi_{r,Rx} = \phi_{r,Tx} + \Delta\phi_{r,H} \quad (A9)$$

$$\phi_{\frac{3}{4},Rx} = \phi_{\frac{3}{4},Tx} + \Delta\phi_{\frac{3}{4},H} \quad (A10)$$

$$\phi_{\frac{3}{5},Rx} = \phi_{\frac{3}{5},Tx} + \Delta\phi_{\frac{3}{5},H} \quad (A11)$$

Since the reference oscillator is fundamentally synchronized with the received reference signal, the phase of its output signal, which is used as the reference of the two RSO is given by:

$$\phi_{5,out} = \phi_{r,Rx} + \phi_5 = \phi_{r,Tx} + \Delta\phi_{r,H} + \phi_5 \quad (A12)$$

where ϕ_5 is constant in time. By properly designing the output network of the reference oscillator, the last expression can be re-written as:

$$\phi_{5,out} = \phi_{r,Rx} = \phi_{r,Tx} + \Delta\phi_{r,H} \quad (A13)$$

At the Rx , the phase of received signals is:

$$\phi_{\frac{3}{4},Rx} = 2\pi f_{o,\frac{3}{4}}t + \phi_{o,\frac{3}{4}} + \frac{1}{4} \left(\phi_r^3 - \Delta\phi_{\frac{3}{4}} \right) + \Delta\phi_{\frac{3}{4},H} \quad (A14)$$

$$\phi_{\frac{3}{5},Rx} = 2\pi f_{o,\frac{3}{5}}t + \phi_{o,\frac{3}{5}} + \frac{1}{5} \left(\phi_r^3 - \Delta\phi_{\frac{3}{5}} \right) + \Delta\phi_{\frac{3}{5},H} \quad (A15)$$

and the phase of the RSO output signals can be expressed as:

$$\phi_{\frac{3}{4},out} = 2\pi f_{o,\frac{3}{4}}t + \phi_{o,\frac{3}{4}} + \frac{1}{4} \left(\phi_r^3 + 3\Delta\phi_{r,H} \right) - \frac{1}{4} \Delta\phi_{\frac{3}{4}} \quad (A16)$$

$$\phi_{\frac{3}{5},out} = 2\pi f_{o,\frac{3}{5}}t + \phi_{o,\frac{3}{5}} + \frac{1}{5} \left(\phi_r^3 + 3\Delta\phi_{r,H} \right) - \frac{1}{5} \Delta\phi_{\frac{3}{5}} \quad (A17)$$

Finally, the received signals and the generated by the receiver RSOs are introduced in two phase comparators, whose outputs are two DC-voltage signals, $V_{\phi,\frac{3}{4}}$ and $V_{\phi,\frac{3}{5}}$, which are proportional to the phase difference between the signals connected to their two inputs.

Mathematically, phase comparators perform the operations (A14)–(A16) and (A15)–(A17). Therefore, its operation is described by:

$$\Delta\Phi_{\frac{3}{4}} = \phi_{\frac{3}{4},Rx} - \phi_{\frac{3}{4},out} = \Delta\phi_{\frac{3}{4},H} - \frac{3}{4}\Delta\phi_{r,H} \quad (\text{A18})$$

$$\Delta\Phi_{\frac{3}{5}} = \phi_{\frac{3}{5},Rx} - \phi_{\frac{3}{5},out} = \Delta\phi_{\frac{3}{5},H} - \frac{3}{5}\Delta\phi_{r,H} \quad (\text{A19})$$

where $\Delta\Phi_{\frac{3}{4}}$ and $\Delta\Phi_{\frac{3}{5}}$ represent the phase difference between the received signals and the provided by the RSOs. Therefore, Equations (A18) and (A19) show the capability of the proposed approach to determine the relative phase change suffered by the transmitted signals.

REFERENCES

1. Mitilineos, S. A., D. M. Kyriazanos, O. E. Segou, J. N. Goufas, and S. C. A. Thomopoulos, "Indoor localization with wireless sensor networks," *Progress In Electromagnetics Research*, Vol. 109, 441–474, 2010.
2. Seow, C. K. and S. Y. Tan, "Localization of omni-directional mobile device in multipath environments," *Progress In Electromagnetics Research*, Vol. 85, 323–348, 2008.
3. Reza, A. W., S. M. Pillai, K. Dimyati, and K. G. Tan, "A novel positioning system utilizing zigzag mobility pattern," *Progress In Electromagnetics Research*, Vol. 106, 263–278, 2010.
4. Liu, H.-Q., H.-C. So, K. W. K. Lui, and F. K. W. Chan, "Sensor selection for target tracking in sensor networks," *Progress In Electromagnetics Research*, Vol. 95, 267–282, 2009.
5. Harabi, F., H. Changuel, and A. Gharsallah, "Direction of arrival estimation method using a 2-L shape arrays antenna," *Progress In Electromagnetics Research*, Vol. 69, 145–160, 2007.
6. Yang, P., F. Yang, and Z. P. Nie, "DoA estimation with sub-array divided technique and interpolated ESPRIT algorithm on a cylindrical conformal array antenna," *Progress In Electromagnetics Research*, Vol. 103, 201–216, 2010.
7. Tayebi, A., J. Gomez, F. M. Saez de Adana, and O. Gutierrez, "The application of ray-tracing to mobile localization using the direction of arrival and received signal strength in multipath indoor environments," *Progress In Electromagnetics Research*, Vol. 91, 1–15, 2009.
8. Lee, J.-H., Y.-S. Jeong, S.-W. Cho, W.-Y. Yeo, and K. S. J. Pister, "Application of the Newton method to improve the accuracy of

- Toa estimation with the beamforming algorithm and the MUSIC algorithm,” *Progress In Electromagnetics Research*, Vol. 116, 475–515, 2011.
9. Alejos, A. V., M. Garcia Sanchez, I. Cuinas, and J. C. G. Valladares, “Sensor area network for active RTLS in RFID tracking applications at 2.4 GHz,” *Progress In Electromagnetics Research*, Vol. 110, 43–58, 2010.
 10. Mtilineos, S. A. and S. C. A. Thomopoulos, “Positioning accuracy enhancement using error modeling via a polynomial approximation approach,” *Progress In Electromagnetics Research*, Vol. 102, 49–64, 2010.
 11. Alvarez, Y., F. Las Heras, and M. R. Pino, “Full-wave method for RF sources location,” *Proceedings of the 2nd Eur. Conf. on Antennas and Propagation*, Vol. 1, 1–5, 2007.
 12. Myoung, S.-S., Y.-J. An, J.-G. Yook, B.-J. Jang, and J.-H. Moon, “A novel 10 GHz super-heterodyne bio-radar system based on a frequency multiplier and phase-locked loop,” *Progress In Electromagnetics Research C*, Vol. 19, 149–162, 2011.
 13. Ver Hoeye, S., L. Gutierrez, S. Sancho, A. Suarez, and P. Gonzalez, “Sub-harmonic and rational synchronization for phase-noise improvement,” *Proc. 31st Eur. Microw. Conference*, Vol. 1, 237–240, 2001.
 14. Ver Hoeye, S., M. G. Corredoiras, M. Fernandez, C. Vazquez, L. F. Herran, and F. Las Heras, “Harmonic optimization of rationally synchronized oscillators,” *IEEE Microwave and Wireless Components Letters*, Vol. 19, No. 5, 317–319, 2009.
 15. Ramirez, F., E. De Cos, and A. Suarez, “Nonlinear analysis tools for the optimized design of harmonic-injection dividers,” *IEEE Transactions on Microwave Theory and Techniques*, Vol. 51, No. 6, 1752–1762, 2003.
 16. Ver Hoeye, S., L. F. Herran, M. Fernandez, and F. Las Heras, “Design and analysis of a microwave large-range phase-shifter based on an injection-locked harmonic self-oscillating mixer,” *IEEE Microwave and Wireless Components Letters*, Vol. 16, No. 6, 342–344, 2006.
 17. Vazquez Antuna, C., S. Ver Hoeye, M. Fernandez Garcia, L. F. Herran Ontanon, and F. Las-Heras Andrés, “Analysis of the performance of injection locked oscillators in a data transmitting polarization agile antenna application,” *Progress In Electromagnetics Research Letters*, Vol. 12, 1–10, 2009.
 18. Ver Hoeye, S., C. Vazquez Antuna, M. Gonzalez Corredoiras, M. Fernandez Garcia, L. F. Herran Ontanon, and F. Las-Heras

- Andrés, “Multi-harmonic DC-bias network based on arbitrarily width modulated microstrip line,” *Progress In Electromagnetics Research Letters*, Vol. 11, 119–128, 2009.
19. Hotopan, G. R., S. Ver Hoeye, C. Vazquez Antuna, R. Cambolor Diaz, M. Fernandez Garcia, F. Las-Heras Andrés, P. Alvarez, and R. Menéndez, “Millimeter wave microstrip mixer based on graphene,” *Progress In Electromagnetics Research*, Vol. 118, 57–69, 2011.
 20. Vazquez, C., S. Ver Hoeye, C. Vazquez, M. Fernandez, L. F. Herran, and F. Las Heras, “Design of a three port triple band aperture coupled microstrip antenna,” *Proceedings of the IEEE Antennas and Propagation Symposium*, Vol. 1, 95–98, 2008.
 21. Chiu, C.-W., C.-H. Chang, and Y.-J. Chi, “Multiband folded loop antenna for smart phones,” *Progress In Electromagnetics Research*, Vol. 102, 213–226, 2010.
 22. Sze, J.-Y. and Y.-F. Wu, “A compact planar hexa-band internal antenna for mobile phone,” *Progress In Electromagnetics Research*, Vol. 107, 413–425, 2010.
 23. Liao, W.-J., S.-H. Chang, and L.-K. Li, “A compact planar multiband antenna for integrated mobile devices,” *Progress In Electromagnetics Research*, Vol. 109, 1–16, 2010.
 24. Ver Hoeye, S., A. Suarez, and S. Sancho, “Analysis of noise effects on the nonlinear dynamics of synchronized oscillators,” *IEEE Microwave and Wireless Components Letters*, Vol. 11, No. 9, 376–378, 2001.
 25. Adler, R., “A study of locking phenomena in oscillators,” *IEEE Proceedings*, Vol. 61, No. 10, 1380–1385, 1973.